Numerical Investigation of Vibration Suppression for the Combined Device of Non-Newtonian Fluids Coupled Elastic Baffle

Y. H. Chen, Y. F. Yue, Y. Zhang, R. P. Li and X. Xu[†]

School of Advanced Manufacturing, Nanchang University, Nanchang 330031, China

†*Corresponding Author Email: xuxun@ncu.edu.cn*

ABSTRACT

Tuned liquid dampers (TLDs) have been broadly applied to suppress structural vibrations. In the present study, a novel vibration mitigation device consisting of non-Newtonian fluids coupled with an elastic baffle is proposed. The fluid-structure interaction is studied numerically. To optimize the system, different fluids, including the Bingham fluid, the Pseudoplastic fluid, and the Dilatant fluid are used as the damping fluids and the vibration suppression ability of each fluid is studied. Moreover, the energy dissipation mechanisms of different liquids are obtained. The results show that the optimal vibration suppression in the container without a baffle can be achieved by using the Bingham fluid. In this case, the average amplitude decay rate of the container is 12.662% with about 0.199% improvement in the damping ratio when compared to water. In the container with an elastic baffle, however, both the Pseudoplastic fluid and the Dilatant fluid outperform water in the damping capacity. The average amplitude decay rates of these fluids are 50.960% and 43.794%, respectively. Moreover, their damping ratios are 0.035% and 0.019% higher than that of water, respectively.

Keywords: Non-Newtonian fluid; Sloshing liquid damping; Elastic baffle; Energy dissipation mechanism; Numerical simulation.

NOMENCLATURE

Fluid #1	water	Model B	container with elastic baffle
Fluid #2	pseudoplastic fluid	T	time
Fluid #3	Bingham fluid	t_{max}	time when $X=X_{max}$
Fluid #4	dilatant fluid	v_{max}	velocity when $X=X_{max}$
F_{wall}	liquid force acting on the wall	X	displacement of container in the horizontal direction
F_{baffle}	liquid force acting on the elastic baffle	X_{max}	maximum value of container displacement
Model A	container without baffle		

1. INTRODUCTION

With increasing urbanization speed in the last few decades, the height of new skyscrapers has increased to save construction space while ensuring aesthetic issues. This may decrease the structural damping and stiffness of buildings, making them more susceptible to damage by strong winds and earthquakes. A tuned liquid damper (TLD) is a low-cost and simple-to-install system, which is widely used to control passive structural vibrations (Konar and Ghosh 2021). TLD mainly consists of a tank containing liquid (often water) that dissipates the vibration energy through liquid boundary layer friction, free surface contamination, and wave breaking (Ashasi-Sorkhabi *et al.* 2017). However, studies show that at too large accelerations of the horizontal excitation, damping capacity of the system decreases significantly, and the sloshing of the fluid in the TLD may not suppress structural vibrations.

Aiming at resolving this shortcoming and improving the energy dissipation capacity of TLD, numerous investigations have been carried out. In this regard, various flow damping structures (FDSs) such as nets (An *et al.* 2019), slat screens (Faltinsen and Timokha 2011; Halabian and Torki 2011; Crowley and Porter 2012; Hamelin *et al.* 2013; Marivani and Hamed 2014; Marivani and Hamed 2017), baffles (Cammelli *et al.* 2016; Meng *et al.* 2020; Wu *et al.* 2021), floating objects (Ruiz *et al.* 2016; Zhang *et al.* 2019), and obstacles at the tank base (Nayak and Biswal 2016; Kargbo *et al.* 2019) have been proposed.

The sloshing phenomenon of non-Newtonian fluid in the container has been widely investigated. Zhang *et al.* (2017) developed a numerical model for non-Newtonian flows and studied the sloshing of nickel ore slurry in a cargo hold. Moreover, the parametric studies of the excitation frequency, excitation amplitude, and depth to width ratio on the sloshing-induced moment were analyzed extensively. The results showed that the maximum sloshing-induced moment occurred in the resonance region. Grossi and Shabana (2018) used nonlinear continuum-based crude oil constitutive models to study the effect of sloshing on the dynamics and stability of a railroad vehicle. It was observed that as the oil viscosity increased, the longitudinal displacement of oil decreased in both ECP braking and conventional braking. The results showed that the use of bulkheads reduced the maximum coupler force by 70%, decreased the amplitude of the sloshing oscillation, and led to an even distribution of the normal contact force on the wheels. Shimanovsky *et al.* (2014) performed finite element analysis and studied the oscillations of Newtonian and non-Newtonian liquids in a cylindrical transport reservoir during braking. In this regard, the characteristics of Newtonian, Ostwald de Waele, and Bingham models of sloshing liquid in the tank with/without internal perforated baffles were analyzed and the relationship between the hydrodynamic pressure and the energy dissipation rate of studied fluids with different filling levels was extracted. Kuzniatsova and Shimanovsky (2015) studied the effect of lateral baffles on the hydrodynamic pressure and energy dissipation rate for different types of liquids in road tanks.

Based on the performed literature survey, it is inferred that the combination of water and FDSs can be effectively applied to dissipate the vibrational energy of buildings, while the combination of FDSs and non-Newtonian fluids is mainly applied in road or marine transportation to suppress the fluid sloshing during the transportation. The main objective of the present study is to propose a coupling energy dissipation system of FDS and non-Newtonian fluids to reduce the response of the building to the power input and dissipate the structural vibrational energy under the action of external excitation.

2. METHODOLOGY

2.1 Physical Model

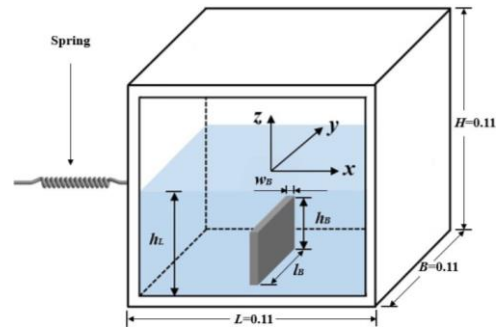The physical model of the system is shown in Fig. 1.

Fig. 1. 3D schematic of the rectangular tank with an internal baffle.

The coordinate origin is at the center of the hydrostatic surface. The model consists of a square steel tank with a wall thickness of 0.005 m and a length of 0.11 m. A horizontal spring is installed between the outer wall of the tank and the ground. The spring stiffness was 8382.8 N/m to achieve a sufficient vibration period and obtain the best vibration suppression effect. A baffle with a 0.09 m long (l_B), 0.045 m high (h_B), and 0.004 m wide (w_B) is mounted in the tank center. The liquid filling ratio of the container is 50% (h_L=0.05 m). The liquid level is 0.005 m higher than the upper surface of the built-in baffle. The container is released from the equilibrium position of 5 mm and is subjected to free decay motion under the influence of the spring.

Vibration attenuation of the combined system mainly depends on the turbulence of the flow and the interaction between the baffle and the fluid. In this section, it is intended to compare the vibration suppression performances of non-Newtonian fluids and water. It is worth noting that the effect of the structural size on the results is ignored.

2.2 Numerical Calculation Method

Vibration of the container forces the fluid to slosh while the fluid interacts with the baffle, this process is a complex mutual effect between the tank and the liquid. The whole process is numerically simulated with an implicit coupling method of partitioned solvers. The meshed domains are presented in Fig. 2. In the solid domain, the finite element method (FEM) is adopted to solve the stress-strain of the structure. The tank and the baffle have one degree of freedom in the horizontal direction. The spring's mass and damping and the contact friction effects between various components are ignored during the calculations. The Navier-Stokes equations are solved in the fluid domain using the finite volume method (FVM). The solid domain and the fluid domain are coupled at the interface. The standard k-Epsilon model is used to simulate the turbulence flow. A second-order backward Euler algorithm is applied to solve the governing equations in the transient format. In this paper, non-Newtonian fluids are assumed to be homogeneous and single-phase.

2.3 Governing Equations

The governing equations for viscous and incompressible non-Newtonian fluids can be
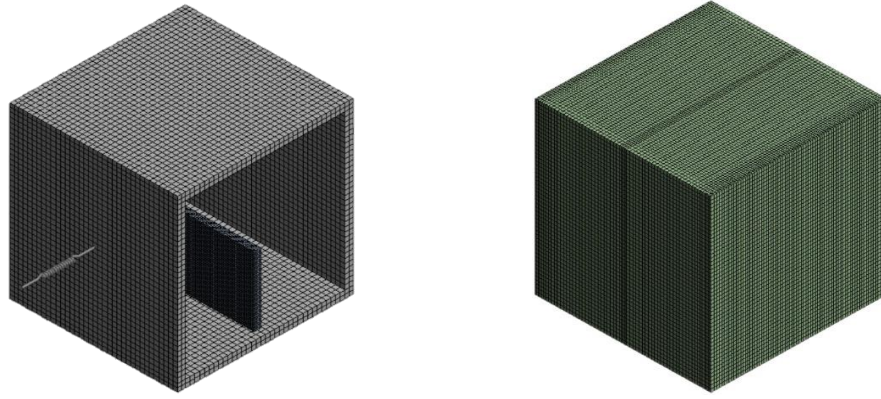
(a) Mesh of the solid domain
(b) Mesh of the Fluid domain

Fig. 2. Meshed domains.

expressed in the form below (Zhang *et al.* 2020):

$$\frac{d\vec{u}}{dt} = \vec{f} - \left(\frac{1}{\rho}\right)\nabla p + \Delta v\vec{u} \tag{1}$$

$$\nabla \cdot \vec{u} = 0 \tag{2}$$

where t, $\vec{u}$, $\vec{f}$, ρ, p and v are the time, velocity vector, external body forces acting on the fluid particles, density, pressure, and kinematical viscosity of the liquid, respectively.

Shear stresses between particles in Newtonian fluids are positively correlated with the relative movement velocity of its layers. This can be mathematically expressed as follows:

$$\tau = \mu\dot{\gamma} \tag{3}$$

where τ is yield stress, $\dot{\gamma}$ is the shear rate, and μ denotes the dynamic viscosity coefficient.

In the present study, the Pseudoplastic model (Li *et al.* 2017), the Bingham model (Sun 2000), and the Dilatant model (Doludenko 2020) are applied to simulate the flow. The correlation between the stress velocity and stress shear of the Bingham model can be expressed as follows (Tang and Lu 2014):

$$\tau - \tau_0 = \mu_P\dot{\gamma}, \tau > \tau_0 \tag{4}$$

where τ_0 is initial shear stress and μ_p is the plastic viscosity of the non-Newtonian fluid.

The Ostwald de Waele model can be used to describe the viscosity of the non-Newtonian fluids based on the shear rate. The dynamic viscosity of this model can be expressed as follows (Kim *et al.* 1983; Tang and Lu 2014):

$$\mu(\dot{\gamma}) = K(\dot{\gamma})^{n-1} \tag{5}$$

where K is the flow rate density and n is the power-law index. When $n<1$ or $n>1$, the model represents the Pseudoplastic fluid or the Dilatant fluid, respectively.

The angular frequency of the spring is calculated from Eq. (6) as 9 Hz.

$$\omega_s = \left(\frac{k}{m_s}\right)^{\frac{1}{2}} \tag{6}$$

where k is the spring stiffness and m_s is the mass of the container.

2.4 Numerical Model

The numerical method is verified by using the results published by Xu *et.al* (2018). The weight of the container is 2.1274 kg and it contains 0.332 kg of water with a standing wave frequency of 2.82 Hz. The initial displacement of the structure is 5 mm. It can be seen that there is a good agreement between the results from Fig. 3.

Three grid resolutions are tested and the displacement response curves are presented in Fig. 4a. It is observed that the attenuation trends in the grid size of 0.002 m and 0.001 m are consistent. The timestep independence verification is shown in Fig. 4b. The hexahedron grid is employed in the study for the simulation. To accurately analyze the flow and the interactions between the fluid and the baffle, refined meshes are used near the boundary layer and the free surface. Considering the computational expenses and computing resources, the mesh size and the time-step are set to 0.002 m and 0.002 s, respectively.
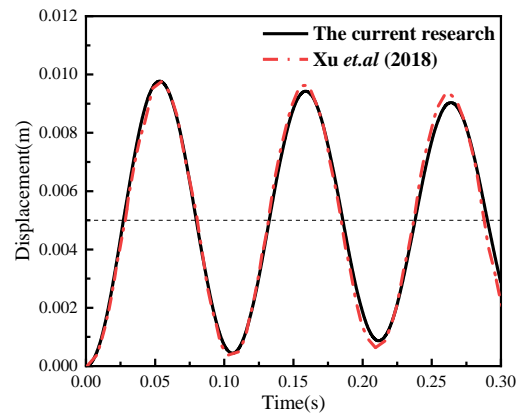

Fig. 3. Model validation

3. RESULTS AND DISCUSSIONS

To simplify the analyses, some parameters are defined as shown in the nomenclature table.

3.1 Attenuation of the Displacement

Figure 5 shows the response curves of the four fluids in models A and B while the tank vibrates horizontally with an amplitude of 0.005 m. Fig. 5a shows that in model A, the response amplitude of fluid #3 has a significant decay compared to fluid #1.

The largest vibration amplitude decay of fluid #1 occurs at t=0.474 s, which is 10.736% lower than the previous peak. Moreover, it is found that the average amplitude decay rate of fluid #3 is 12.662%. Compared with water, the damping ratio of the Bingham fluid is improved by 0.199%. It is inferred that the best vibration suppression performance in the container without a baffle (model A) can be achieved using fluid #3 (Bingham fluid). Accordingly, the application of fluid #3 improves the damping ratio of the system, but the damping effect of the system without a baffle is not good regardless of the fluid type.
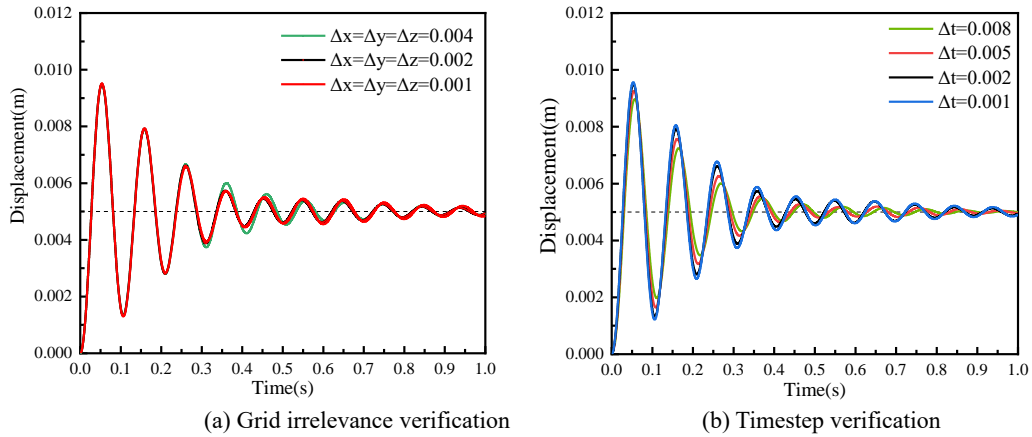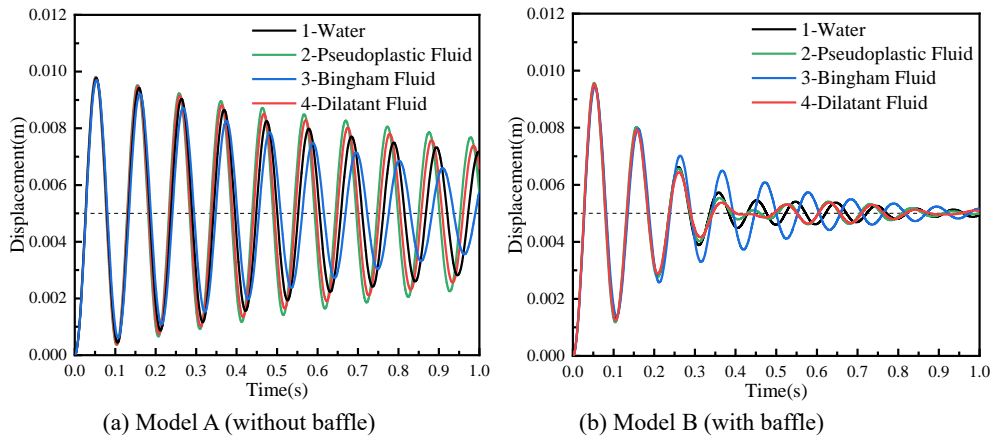

(a) Grid irrelevance verification   (b) Timestep verification

Fig.4. Irrelevance validation

(a) Model A (without baffle)   (b) Model B (with baffle)

Fig. 5. Displacement response curves

(a) Model A (without baffle)   (b) Model B (with baffle)
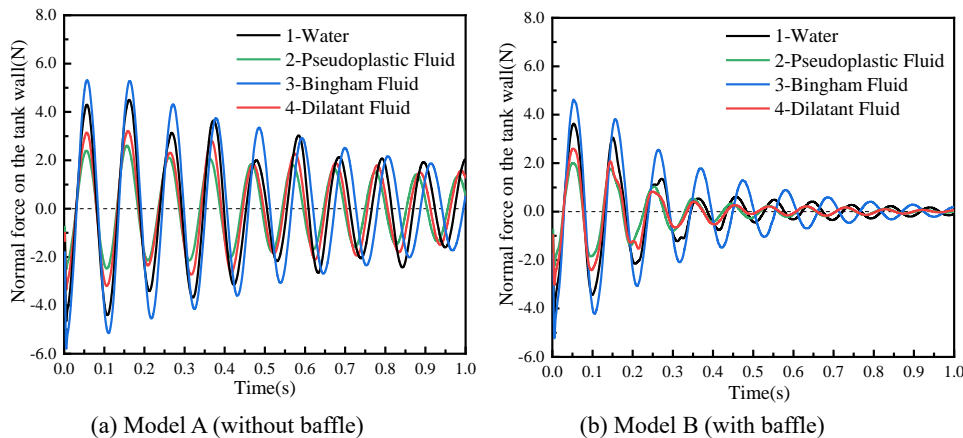
Fig. 6. Normal forces on the container wall (F_{wall}) in two systems with different fluids.

(a) Fluid #1 (Water)

(b) Fluid #2 (Pseudoplastic fluid)

(c) Fluid #3 (Bingham fluid)
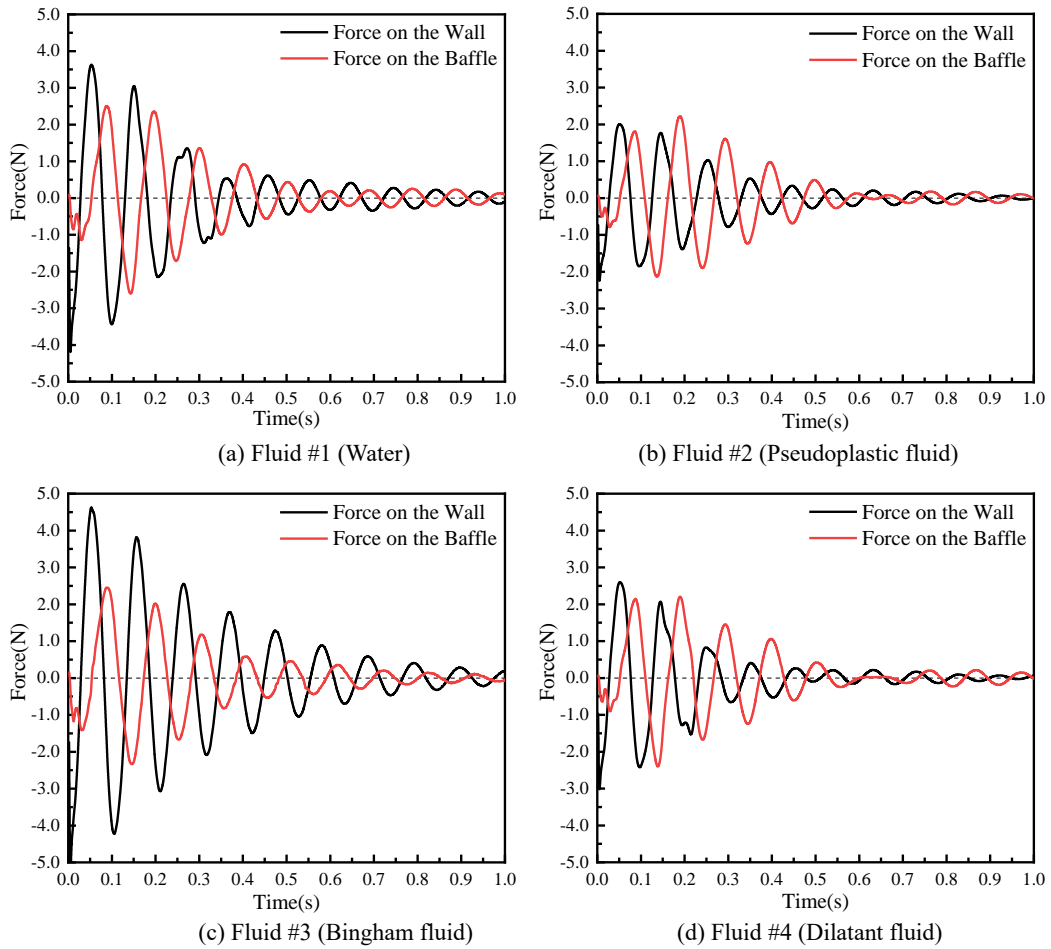
(d) Fluid #4 (Dilatant fluid)

Fig. 7. Distributions of F_{wall} and F_{baffle} in model B for different fluids.

Figure 5b shows that in model B, the response curves of fluids #2 and #4 decay faster than that of fluid #1.

On the other hand, fluid #3 has a relatively slow attenuation of the response curve and the worst vibration suppression effect on the container. Therefore, fluid #3 is not an appropriate choice and will not be discussed here. During the period from 0.36 s to 0.53 s, the displacements of fluids #2 and #4 are around 0.005 m and the vibration positions of these two systems are very close to the equilibrium position. It is concluded that fluids #2 and #4 respond quickly to the excitation. However, the decay rate of fluid #1 decreases with no significant difference between the two adjacent displacement peaks. After 0.53 s, the response curves of fluids #2 and #4 increase first and then decrease. Finally, they gradually approach the equilibrium position. The average decay rates of the response curves of fluids #1, #2, and #4 are 31.161%, 50.960%, and 43.794%, respectively. Compared with water, the damping ratios of fluids #2 and #4 are improved by 0.035% and 0.019%, respectively.

3.2 Normal Force on the Wall

Figure 6 shows the normal forces acting on the container wall (F_{wall}) by the fluids in different systems. It is worth noting that these forces originate from the

liquid particles hitting the wall during the sloshing process. The magnitude of F_{wall} is related to the liquid properties and the excitation amplitude. In model A, the energy is dissipated mainly by the impact of the fluid on the wall. Fluid #2 has initial shear stress and is more viscous than water so exerts a larger force on the wall. Moreover, the response of the sloshing fluid to the excitation has a delay compared to that of the container, which hinders the movement of the container and suppresses its vibration. The maximum and minimum values of F_{wall} of fluid #3 along the positive direction are 5.324 N and 1.879 N, respectively. Furthermore, the maximum and minimum values of F_{wall} along the negative direction are -5.870 N and -1.734 N, respectively. At t=0.272 s, the maximum decay amplitude of F_{wall} is 0.970 N.

In Model B, vibrational energy is dissipated by the fluid acting on the wall, and the interaction between the fluid and the elastic baffle. Therefore, the energy dissipation mechanism of model B cannot be explained based on F_{wall} alone. This issue is further discussed in the following section.

3.3 The Comparison of F_{wall} and F_{baffle}

The comparison of F_{wall} and F_{baffle} for different fluids is presented in Fig. 7. The magnitude of F_{baffle} depends on the rheological characteristics of the fluid

and the interaction degree between the fluid and the baffle.

Figure 7 reveals that F_{wall} values of fluids #1, #2, and #4 are gradually slightly than their F_{baffle} values, indicating that the interaction between these three fluids and the elastic baffle is sufficient. In Model B, the energy transferred to the container by the excitation is mainly dissipated through the interaction between the fluid and the elastic baffle. Fig. 7 also shows that the F_{wall} of fluid #3 is greater than its F_{baffle}, indicating that the interaction between fluid #3 and the elastic baffle is very weak, and the system mainly suppresses the vibration through the reaction force generated by the fluid impacting the wall.

The F_{baffle} of fluid #1 is significantly larger than its F_{wall} only at the fourth peak and then decreases gradually because of the energy dissipation. The F_{baffle} of fluids #2 and #4 is significantly larger than F_{wall} after the second peak, indicating that these fluids respond quickly to the excitation. Moreover, the F_{baffle} of fluids #2 and #4 are larger than the corresponding F_{wall} in the period of 0.2 s~0.5 s. It is concluded that the interaction between the fluid and the elastic baffle is the dominant energy dissipation mechanism during this period. When F_{wall} is smaller than F_{baffle}, the maximum absolute difference (i.e. $| F_{baffle} - F_{wall} |_{max}$) of fluids #1, #2, and #4 are 0.385 N, 0.581 N, and 0.651 N, respectively. It should be indicated that each fluid has specific rheological properties so the force curves are different in terms of fluctuation period, decay amplitude, and stability. In addition, the excitation is transferred from the container to the fluid, and then from the sloshing fluid to the baffle. Therefore, the response curve of F_{baffle} lags behind that of F_{wall}.

3.4 Analysis of the Liquid Flow

Figures 8 and 9 show the two-phase distributions in the tank and the velocity distribution of the flow field at $X=X_{max}$ in models A and B, respectively. In this section, only fluids with better damping effects than water (fluid #1) are discussed.

Figure 5a shows that the response curve of fluid #3 in model A is slightly lower than that of fluid #1 in the 1st cycle. In subsequent cycles, the attenuation amplitude of fluid #3 gradually increases compared to that of fluid #1. Fig. 8 illustrates the liquid flows of fluid #1 and fluid #3 at peak displacements from the 1st to the 4th cycles. Within this period, t_{max} for the fluid #1 is 0.054 s，0.106 s，0.158 s，0.212 s, 0.264 s, 0.316 s, 0.370 s and 0.422 s, while t_{max} for the fluid #3 is 0.054 s，0.108 s，0.160 s，0.214 s，0.268 s, 0.322 s, 0.376 s and 0.428 s, respectively.

Table 1 shows that the velocity magnitudes of fluids #1 and #3 are approximately equal at 0.054 s. However, the velocity of fluid #3 is significantly lower than that of fluid #1 after t=0.106 s. Values of v_{max} for these two fluids in the 1st cycle are shown in Table 1. Moreover, Fig. 8 illustrates that strong liquid sloshing happens in fluid #1 and its horizontal motion is more severe than in fluid #3. Crests and wave breaks are generated as fluid #1 hits the wall and during the reverse flow. Variations of the free surface

Table 1 v_{max} value in the 1st cycle

Fluid	In the positive direction		In the negative direction	
	t /s	v_{max} /(m·s^{-1})	t /s	v_{max} /(m·s^{-1})
1	0.054	0.254	0.106	0.475
3	0.054	0.211	0.108	0.095

in fluid #3 are smoother and more restrictive than that of fluid #1, and the velocity of fluid #3 is always lower than that of fluid #1. This may be attributed to the inherent properties of fluid #3. This type of fluid flow requires certain initial stress to initiate, otherwise, it acts as a solid. When the container vibrates, some energy is consumed by driving the flow of fluid #3. Therefore, the energy carried by the fluid when it starts to flow is less than the total energy transferred to the container from the external source of excitation (Korobeinikov 2000; Zhang *et al*. 2016; Shamsoddini and Abolpour 2021).

Figure 5b shows that in model B, the peak displacements of fluids #2 and #4 are slightly higher than that of fluid #1 in the 2nd cycle, decays from the 3rd cycle, and the highest displacement reduction occurs in the 5th cycle. Fig. 9 shows the flows of these three fluids in the 2nd to 5th cycles.

In the 2nd cycle, fluids #2 and #4 respond rapidly to the excitation and the disturbance is generated at the top of the baffle. Table 2 shows the v_{max} value of these three fluids during this cycle.

During the vibration process, the baffle's bending degree illustrates interactions between the baffle and the fluid. Fig. 9a shows the wave breaking near the wall, liquid backflow originating from the container vibration, and the flow disturbance caused by the swing of the baffle. It is observed that when the flow field velocity decreases after 0.406 s, these phenomena diminish or disappear.

Figure 9b demonstrates that the energy of the system is dissipated mainly through the vortex generated at the top of the baffle. In the initial stage, a large external excitation increases the velocity gradient inside the fluid, which increases the shear rate of the fluid instantaneously and increases instability (Li *et al.* 2016) of fluid #2. Therefore, fluid #2 is highly susceptible to the swing influence of the baffle and a vortex appears at the top of the baffle.
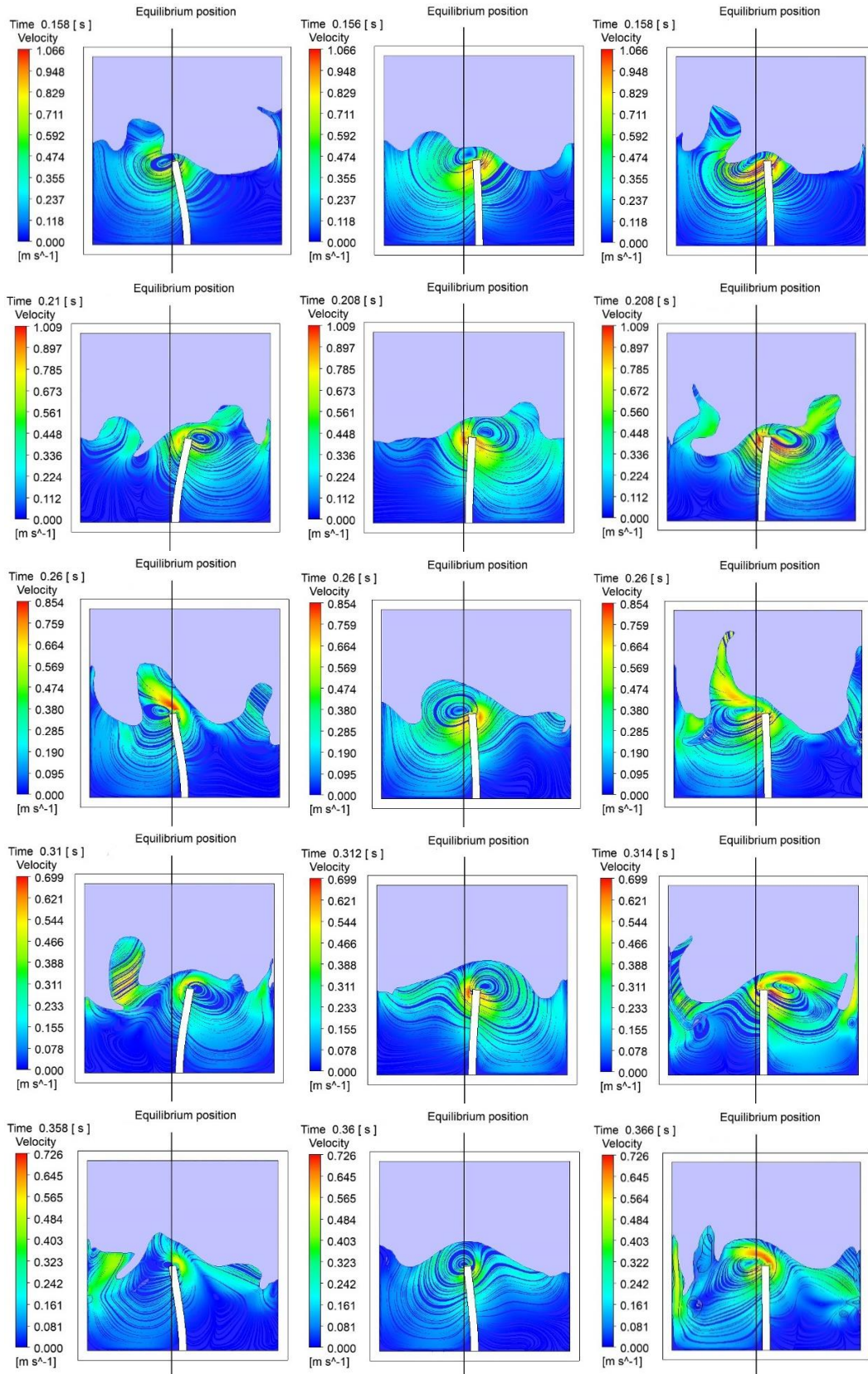
Table 2 v_{max} value in the 2nd cycle

Fluid	In the positive direction		In the negative direction	
	t /s	v_{max} /(m·s^{-1})	t /s	v_{max} /(m·s^{-1})
1	0.158	0.779	0.210	0.875
2	0.156	0.987	0.208	1.009
4	0.158	1.066	0.208	1.009
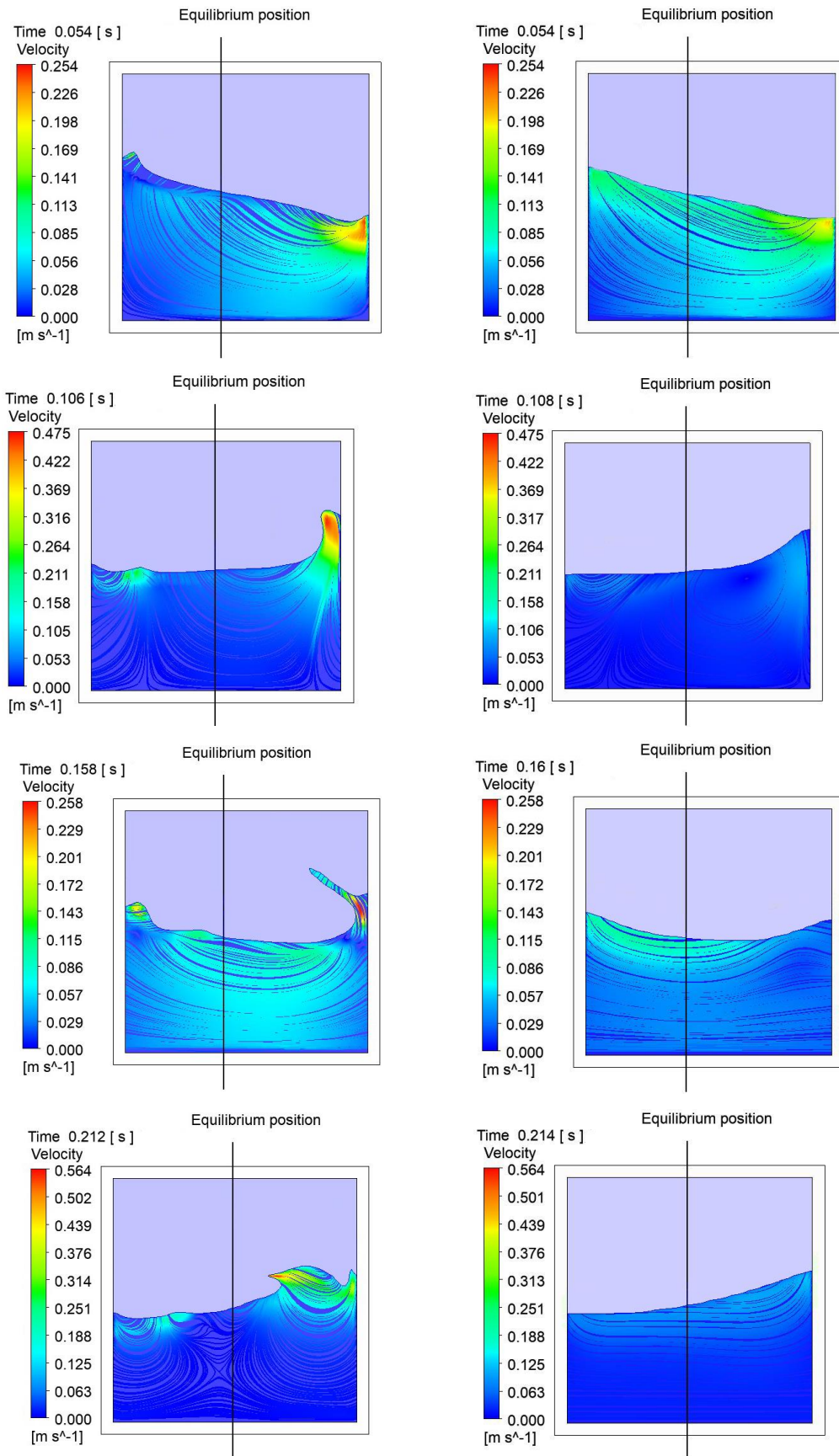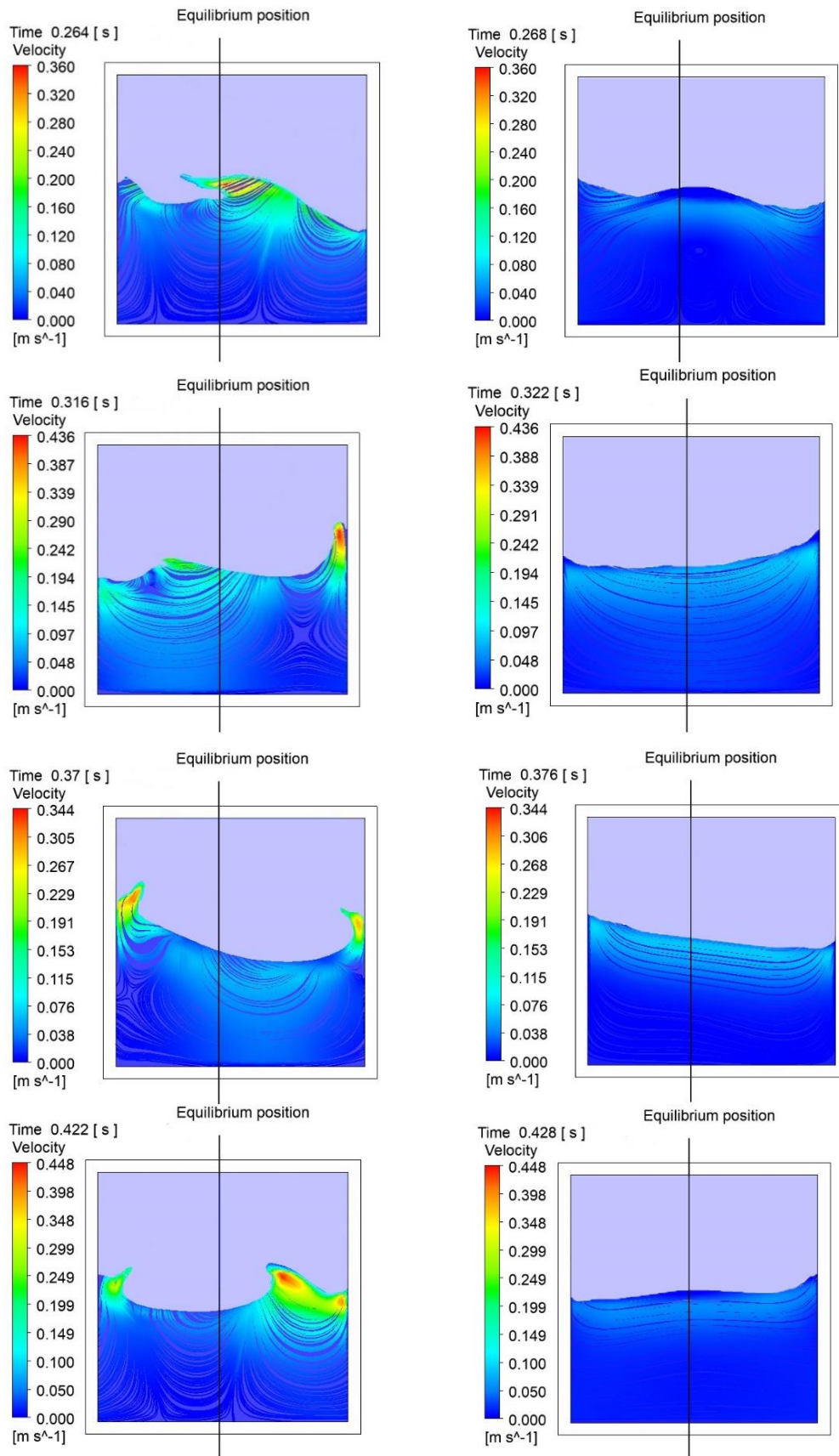
(a) Fluid #1(Water)   (b) Fluid #3 (Bingham fluid)
Fig. 8. The comparison of the liquid flow in model A for different fluids.

(a) Fluid #1 (Water)   (b) Fluid #2 (Pseudoplastic fluid)   (c) Fluid #4 (Dilatant fluid)
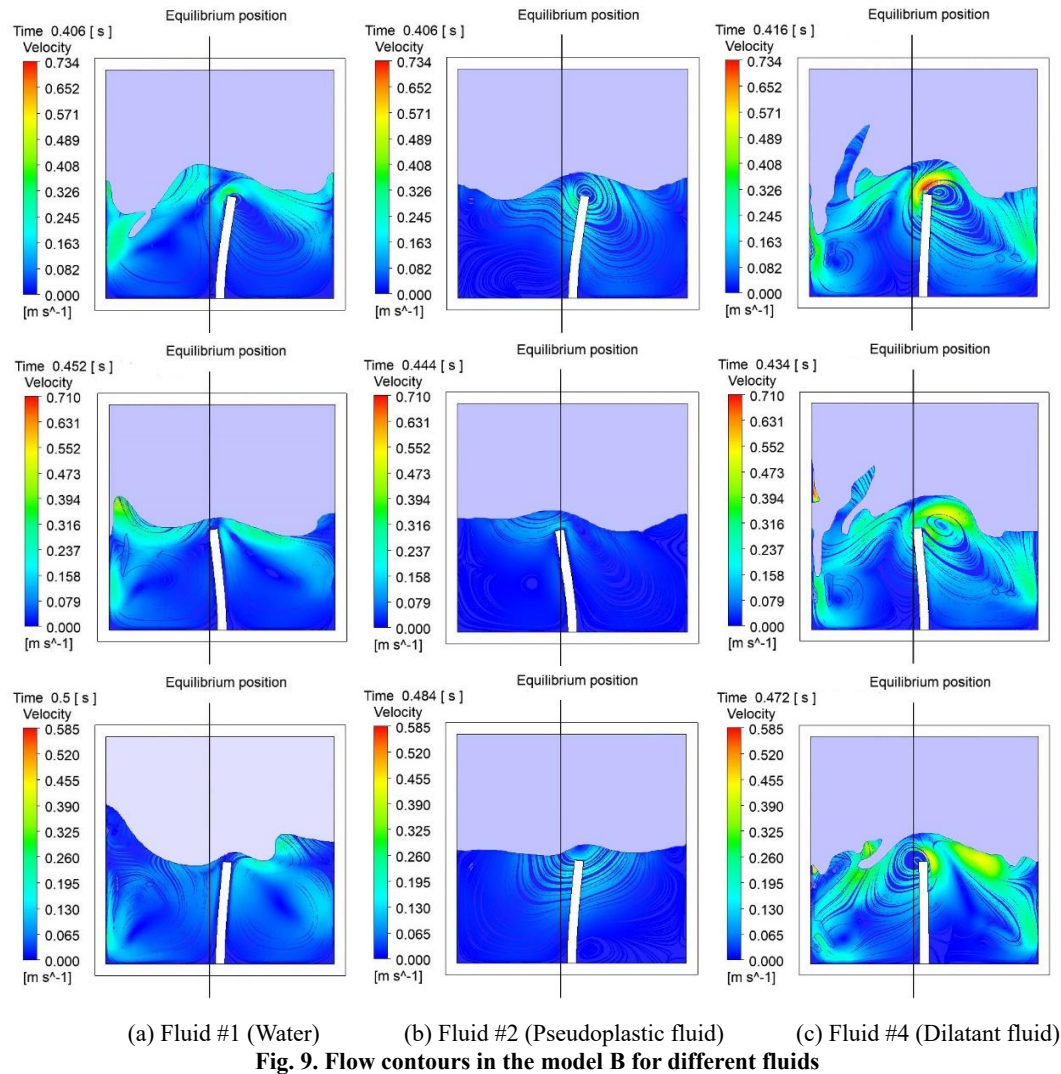**Fig. 9. Flow contours in the model B for different fluids**

Figure 9c shows that the free surface of fluid #4 is severely broken and the fluid near the wall even "climbs up" along the wall. The top of the baffle has a long duration of disturbance to the fluid and a wide range of action. The transient excitation affects the properties of fluid #4. With the continuous decay of the excitation, the flow of fluid #4 reversibly progresses towards shear thinning.

4. CONCLUSION

In the present study, a novel vibration suppression system is proposed. The system is based on sloshing non-Newtonian liquids with an elastic baffle. To evaluate the vibration suppression performance of the system, numerical simulations are carried out and microflows of these fluids are analyzed. From the simulation results we can conclude that

(1) In the system without a baffle, the best vibration suppression performance can be achieved from the Bingham fluid (fluid #3), where some energy is consumed to overcome the initial shear stress and drive the fluid flow. When using the Bingham fluid as the damping liquid, the excitation of the fluid flow requires a large

energy input. The average amplitude decay rate of the structure is 12.662% with about 0.199% improvement in the damping ratio when compared to water.

(2) In the system with an elastic baffle, both the Pseudoplastic fluid (fluid #2) and the Dilatant fluid (fluid #4) have better vibration mitigation performances than water. Moreover, both fluids have rapid responses to external excitation. When applying these two fluids as the damping liquid, the average decay rate of the response curve is 50.960% and 43.794%, respectively. Their damping ratios are 0.035% and 0.019% higher than that of water, respectively. In the 2nd cycle, fluids #2 and #4 respond rapidly to the excitation and the disturbance is generated at the top of the baffle. It is found that the flow instability of the Pseudoplastic fluid increases the shear rate and the energy dissipation by the vortex, which forms at the top of the baffle. The flow of the Dilatant fluid develops reversibly towards shear thinning after being transiently excited. The energy is dissipated by wave breaking on the free surface and by disturbances generated at the top of the baffle.

The performed analyses demonstrate that under simple harmonic vibrations, the vibration suppression performance of the proposed system with an internal elastic baffle immerged in a non-Newtonian fluid outperforms the capacity of the conventional TLD with water as the damping liquid. This study provides a reference for the application of non-Newtonian fluids in vibration suppression.

REFERENCES

An, Y. H., A. M. Asce, Z. Z. Wang, G. Ou, S. S. Pan and J. P. Ou (2019). Vibration Mitigation of Suspension Bridge Suspender Cables Using a Ring-Shaped Tuned Liquid Damper. *Journal of Bridge Engineering* 24(4), 04019020.

Ashasi-Sorkhabi, A., H. Malekghasemi, A. Ghaemmaghami and O. Mercan (2017). Experimental investigations of tuned liquid damper-structure interactions in resonance considering multiple parameters. *Journal of Sound and Vibration* 388, 141-153.

Cammelli, S., Y. F. Li and S. Mijorski (2016). Mitigation of wind-induced accelerations using Tuned Liquid Column Dampers: Experimental and numerical studies. *Journal of Wind Engineering and Industrial Aerodynamics* 155, 174-181.

Crowley, S. and R. Porter (2012). An analysis of screen arrangements for a tuned liquid damper. *Journal of Fluids and Structures* 34, 291-309.

Doludenko, A. N. (2020). Experimental and numerical investigation of the Rayleigh-Taylor instability of the Newtonian and dilatant fluid system. *Physica Scripta* 95(11), 115207.

Faltinsen, O. M. and A. N. Timokha (2011). Natural sloshing frequencies and modes in a rectangular tank with a slat-type screen. *Journal of Sound and Vibration* 330(7), 1490-1503.

Grossi, E. and A. A. Shabana (2018). ANCF analysis of the crude oil sloshing in railroad vehicle systems. *Journal of Sound and Vibration* 433, 493-516.

Halabian, A. M. and M. Torki (2011). Numerical studies on the application of tuned liquid dampers with screens to control seismic response of structures. *The Structural Design of Tall and Special Buildings* 20(2), 121-150.

Hamelin, J. A., J. S. Love, M. J. Tait and J. C. Wilson (2013). Tuned liquid dampers with a Keulegan-Carpenter number-dependent screen drag coefficient. *Journal of Fluids and Structures* 43, 271-286.

Kargbo, O., M. A. Xue and J. H. Zheng (2019). Multiphase sloshing and interfacial wave interaction with a baffle and a submersed block. *Journal of Fluids Engineering* 141(7).

Kim, H. W., D. R. Jeng and K. J. DeWitt (1983). Momentum and heat transfer in power-law fluid flow over two-dimensional or axisymmetrical bodies. *International Journal of Heat and Mass Transfer* 26(2), 245-259.

Konar, T. and A. D. Ghosh (2021). Flow damping devices in tuned liquid damper for structural vibration control: a review. *Archives of Computational Methods in Engineering* 28(4), 2195-2207.

Korobeinikov, A. (2000). Numerical simulation of the oscillations of non-newtonian viscous fluids with a free surface. *Journal of Applied Mathematics and Decision Sciences* 4(2), 111-123.

Kuzniatsova, M. G. and A. O. Shimanovsky (2015). Comparative Analysis of Forms of Lateral Baffles for Road Tanks. *Applied Mechanics and Materials* 797, 290-298.

Li, P., D. Zhang, Y. H. Xie and G. N. Xie (2016). Flow structure and heat transfer of non-Newtonian fluids in microchannel heat sinks with dimples and protrusions. *Applied Thermal Engineering* 94, 50-58.

Li, S. N., H. N. Zhang, X. B. Li, Q. Li, F. C. Li, S. Z. Qian and S. W. Joo (2017). Numerical study on the heat transfer performance of non-Newtonian fluid flow in a manifold microchannel heat sink. *Applied Thermal Engineering* 115, 1213-1225.

Ma, C. L., C. W. Xiong and G. W. Ma (2021). Numerical study on suppressing violent transient sloshing with single and double vertical baffles. *Ocean Engineering* 223, 108557.

Marivani, M. and M. S. Hamed (2014). Numerical Study of Slat Screen Pattern Effect on Design Parameters of Tuned Liquid Dampers. *Journal of Fluids Engineering* 136(6).

Marivani, M. and M. S. Hamed (2017). Evaluate pressure drop of slat screen in an oscillating fluid in a tuned liquid damper. *Computers and Fluids* 156, 384-401.

Meng, X., D. Zhou, M. K. Kim and Y. M. Lim (2020). Free vibration and dynamic response analysis of liquid in a rectangular rigid container with an elastic baffle. *Ocean Engineering* 216, 108119.

Nayak, S. K. and K. C. Biswal (2016). Nonlinear seismic response of a partially-filled rectangular liquid tank with a submerged block. *Journal of Sound and Vibration* 368, 148-173.

Ruiz, R. O., A. A. Taflanidis and D. Lopez-Garcia (2016). Characterization and design of tuned liquid dampers with floating roof considering arbitrary tank cross-sections. *Journal of Sound and Vibration* 368, 36-54.

Shamsoddini, R. and B. Abolpour (2021). Bingham fluid sloshing phenomenon modelling and investigating in a rectangular tank using SPH method. *Ships and Offshore Structures* 16(5), 557-566.

Shimanovsky, A., M. Kuzniatsova and A. Sapietová (2014). Modeling of Newtonian and Non-Newtonian Liquid Sloshing in Road Tanks while

Braking. *Applied Mechanics and Materials* 611, 137-144.

Sun, L. M., T. Kikuchi, Y. Goto and M. Hayashi (2000). Tuned liquid damper (TLD) using heavy mud. *Doboku Gakkai Ronbunshu* 2000(661), 211-220.

Tang, G. H. and Y. B. Lu (2014). A resistance model for Newtonian and power-law non-Newtonian fluid transport in porous media. *Transport in Porous Media* 104(2), 435-449.

Wu, J. R., W. K. Zhong, J. Y. Fu, C. T. Ng, L. Y. Sun and P. Huang (2021). Investigation on the damping of rectangular water tank with bottom-mounted vertical baffles: Hydrodynamic interaction and frequency reduction effect. *Engineering Structures* 245, 112815.

Xu, X., T. Guo, G. J. Li, G. Sun, B. Shang and Z. Guan (2018). A combined system of tuned immersion mass and sloshing liquid for vibration suppression: Optimization and characterization. *Journal of Fluids and Structures* 76, 396-410.

Zhang, C. W., P. Su and D. Z. Ning (2019). Hydrodynamic study of an anti-sloshing technique using floating foams. *Ocean Engineering* 175, 62-70.

Zhang, J. W., W. Q. Wu and J. Q. Hu (2017). Parametric studies on nickel ore slurry sloshing in a cargo hold by numerical simulations. *Ships and Offshore Structures* 12(2), 209-218.

Zhang, J. W., W. Q. Wu and J. Q. Hu (2016). A numerical study of the effects of the longitudinal baffle on nickel ore slurry sloshing in a prismatic cargo hold. *Marine Structures* 46, 149-166.

Zhang, Z. L., M. S. U. Khalid, T. Long, J. Z. Chang and M. B. Liu (2020). Investigations on sloshing mitigation using elastic baffles by coupling smoothed finite element method and decoupled finite particle method. *Journal of Fluids and Structures* 94, 102942.